Environmental Science Nano

ROYAL SOCIETY OF CHEMISTRY

PAPER

View Article Online
View Journal | View Issue

Check for updates

Cite this: *Environ. Sci.: Nano*, 2024, **11**, 1487

Selective metal recovery by mucin: turning gold from wastewater into a peroxymonosulfate-activated catalyst†

Shira Gavriely,[ab] Shachar Richter *[ab] and Ines Zucker *[bcd]

Received 1st October 2023,
Accepted 18th February 2024

DOI: 10.1039/d3en00699a

rsc.li/es-nano

The growing volumes of metal wastewater produced by industry require more efficient techniques for metal recovery. Biosorption is an attractive and desirable method for metal recovery because it avoids the additional chemicals beyond the sorbent. Mucin glycoprotein is a natural bioresource that can potentially adsorb and reduce precious metals. In this study, we examine the ability of mucin to recover gold from a mixed-metals solution in an acidic environment modeling industrial wastewater. We show that selectivity in the adsorption of the metals—and particularly precious metals—is driven by the metal's chemical properties and affinity to mucin. The ability of mucin to reduce gold ions and transform them into nanoparticles was also investigated both in mixed-metal solutions and isolated-metal solutions and with two different forms of mucin (dissolved and nanofibers). Lastly, the recovered gold NPs were used in persulfate activation for the oxidation of an organic pollutant: bisphenol A. This study illustrates a two-step circular-economy process—sorption of precious metals and utilizing those adsorbed metals for secondary decontamination—using the benign, cost-effective biomaterial mucin.

Environmental significance

This research demonstrates a two-step process utilizing a benign, cost-effective biomaterial resource named mucin. This unique glycoprotein could adsorb and transform metal ions in wastewater into a useful nano-catalyst which can be used for oxidation of organic pollutants. The process steps exhibited selectivity, from the exclusive recovery of gold from a mixture of metals, to the degradation of bisphenol A in a non-radical persulfate activation. Overall, this process enables decontamination while regenerating precious resources, showcasing this design as a prime example of the nano circular economy framework.

1. Introduction

The rapid growth of modern industry is driving increased wastewater production. In fact, 22% of the freshwater withdrawn globally every year is used by industry and could eventually return as industrial effluents.[1] Of particular concern in certain industrial wastewaters are heavy and precious metals originating in many industrial processes (*e.g.*, jewelry production, electronics, batteries, fuel cells, electroplating resources, medical equipment, and pharmaceuticals).[2,3] These non-degradable metals in wastewater pose an environmental risk by permeating living species through the food chain, bioaccumulating, and causing severe damage to health functions.[4,5] Also, the recovery of precious metals from wastewater holds high economic value. As natural mineral resources are gradually decreasing, recovery of these metals from secondary sources (such as industrial wastewater, discarded electronics, and electroplating waste) has increasingly drawn the attention of researchers.[6–8]

Some current and widely used methods for metal recovery from industrial wastewater are chemical precipitation, filtration, coagulation, photocatalysis, electrodeposition, ion exchange resin, solvent extraction, and reduction.[9–11] The disadvantages of some of these methods are their high cost, low efficiency, limited selectivity, weak efficiency at low ion concentrations, and their need for extensive labor and time.[12] Furthermore, in some of these technologies (such as chemical reduction or solvent extraction),[13] large quantities of wastewater stream are generated upon additions of the chemical agents used for remediation.[14] Therefore, there is a

[a] *Department of Materials Science and Engineering, Faculty of Engineering, Tel Aviv University, Tel Aviv 6997801, Israel. E-mail: srichter@tauex.tau.ac.il; Tel: (+972) 73 3804581*
[b] *Tel Aviv University Center for Nanoscience and Nanotechnology, Tel Aviv 6997801, Israel*
[c] *School of Mechanical Engineering, Faculty of Engineering, Tel Aviv University, Tel Aviv 6997801, Israel. E-mail: ineszucker@tauex.tau.ac.il; Tel: (+972) 73 3804581*
[d] *The Porter School of Environmental and Earth Sciences, Tel Aviv University, 6997801, Israel*

† Electronic supplementary information (ESI) available. See DOI: https://doi.org/10.1039/d3en00699a

need to develop a low-cost and eco-friendly process to recover these precious metals.

In recent decades, the ongoing trend is using biomaterials that can selectively and efficiently adsorb metal ions *via* various physiochemical interactions.[15–17] This green approach allows adsorption even at low metal concentrations, reduce material cost, and elimination of the use of other harmful substances and the creation of by-products.[12,14,18,19] Furthermore, some of these biomaterials can also reduce metal ions while forming metal nanoparticles (NPs) in a green synthesis reaction, often occurring spontaneously (*i.e.*, without external stimuli such as reagents, heat, or light).[20,21] This combined biosorption and bio-reduction process holds excellent potential for benign metal recovery, with the resultant sorbent/sorbate pairing subsequently having direct catalysis applicability.

Our previous studies indicate that mucin glycoprotein can be used as a biomaterial for wastewater remediation.[22–24] Mucin is a large extracellular glycoprotein and the building block of biological mucus, a semi-permeable viscous mesh[25] with a primary role of protecting organs by blocking harmful environmental particle molecules and pathogens.[26,27] Mucin can be extracted from various living sources, including mammals (*e.g.*, pig or bovine) and non-mammals (*e.g.*, snails, worms, or jellyfish),[28,29] and is commonly produced as a by-product in the meat industry.[25,30,31] The core protein in the mucin structure is composed of a vast number of repeated amino acids and contains cysteine-rich domains in the molecule's terminals.[25] Mucin has been previously demonstrated as an efficient and selective biosorbent for mercury ions (rather than other cations like calcium and sodium), which is not surprising, as this sort of selective sorption is one of mucin's natural roles in the natural mucus layer.[23] These mucin characteristics were studied in different living organisms, such as fish, snails, and the human body.[32,33]

Importantly, mucin has also been shown to participate in a bio-assisted synthesis of metal ion-derived NPs within the mucin structure (particularly, with gold, palladium, and silver).[28,34,35] It is assumed that the cysteine amino acid in mucin's molecule can serve as a reduction agent, as its thiol groups can reduce metal ions.[36] Mucin can also serve as the scaffold for NPs formed on the mucin surface, which affects the NP structure and size and stabilizes the NPs from aggregating. The solution conditions, such as pH, can also influence the overall structure of the NPs.[37]

In this respect, metal NPs are often used in various medical applications, optics, electronics, and agriculture fields.[38] In addition, metal NPs can facilitate catalytic or photocatalytic reactions; thus, they can be utilized for energy applications.[39] One highly studied catalytic reaction is persulfate (PS) or peroxymonosulfate (PMS) activation, in which metal NPs are utilized to oxidize and degrade organic contaminants.[40] This reaction is facilitated *via* two different mechanisms depending on the type of metal. In the first—and more understood one—transition metal NPs such as Fe, Co, Cu, and Mo activate PMS to produce highly reactive sulfate radicals ($SO_4^{\cdot-}$), which oxidize and decompose organic compounds.[41] The second—and less understood—PMS activation mechanism with noble metal NPs such as Rh, Pd, and Au. These metals mediate direct electron transfer from the organic compound (electron donor) to persulfate (electron acceptor) to achieve persulfate-driven oxidation without involving the formation of reactive radical species (such as sulfate radicals).[42,43] The latter mechanism was shown to be efficient primarily for phenolic compound degradation, allowing a selective reaction.[44]

In this study, we leverage mucin's ability to selectively adsorb and reduce metals present in an aqueous mixture (Au, Pd, Fe, Cu, Al), and then use the resulting NP–mucin composite as a catalyst. We observe a distinct selective recovery of Au from synthetic wastewater and spontaneous generation of its NPs on the mucin surface (Au@mucin). The Au@mucin composite was further utilized as a catalyst for the activation of persulfate through an electron-transfer mediation mechanism for the degradation of the organic pollutant bisphenol A (BPA). Herein, we transform metal waste into a valuable catalyst for eliminating additional waste (in the form of the organic pollutants), all supported by the green, benign, and sustainable material mucin.

2. Materials and methods

2.1 Chemicals and reagents

Mucin from the porcine stomach (pig gastric mucin, PGM type II, Sigma-Aldrich) was used as purchased. Polycaprolactone (PCL, Mn 80 000, Sigma-Aldrich) was used for the synthesis of mucin-based nanofibers. The following salts were used for selectivity experiments: palladium(II) chloride ($PdCl_2$, Sigma-Aldrich), iron(II) chloride tetrahydrate ($FeCl_2$, Sigma-Aldrich), iron(III) chloride ($FeCl_3$, Sigma-Aldrich), gold(III) chloride ($HAuCl_4$ Sigma-Aldrich), copper(II) nitrate trihydrate ($Cu(NO_3)_2{\cdot}3H_2O$, Strem Chemicals) and aluminum nitrate nonahydrate ($Al(NO_3)_3{\cdot}9H_2O$, Alfa Aesar). Humic acid (Alfa Aesar) and carbamazepine (CBZ, Sigma-Aldrich) were used. Sodium hydroxide (NaOH, 98.5%, Acros) was used for pH adjustments. The background ion solutions were made with calcium chloride ($CaCl_2$, Acros), sodium chloride ($NaNO_3$, Sigma-Aldrich), and potassium chloride (KCl, Acros). Ethylenediaminetetraacetic acid disodium salt dihydrate (99%, $EDTA{\cdot}Na_2{\cdot}2H_2O$, Acros) was used for metal desorption. Oxone (potassium peroxymonosulfate, PMS, Thermo Scientific), bisphenol A (BPA, Sigma Aldrich), 4-chlorobenzoic acid (*p*CBA, Acros), sodium bicarbonate ($NaHCO_3$, Alfa Aesar), and methanol (100% Bio-lab), were used for catalysis experiments. Nitric acid (HNO_3 66–68%, Acros) and hydrochloric acid (HCl 37%, Acros) were used for metal quantification.

2.2 Metal adsorption and selectivity experiments using mucin

In the kinetic adsorption experiments, 500 μL of 10 mg mL^{-1} (5 mg) of PGM solution was added to 50 mL of 0.05 mM metal solution (Au^{3+}, Pd^{2+}, Fe^{2+}, Al^{3+}, or Cu^{2+}). The

adsorption capacity was measured for each metal in isolation and all metals in combination. The tubes were fixed to an orbital shaker rotating at 150 rpm at room temperature. In kinetic experiments, PGM was added to 0.05 mM of the mixed-metal solution and to 0.025, 0.05, 0.1 mM of the Au solution. The effect of background ions on adsorption was estimated in a similar batch adsorption experiment for 0.05 mM Au in the presence of 5 mM of Na^+, Ca^{2+}, and K^+, representing environmentally relevant concentrations in wastewater.[45,46] The effect of organic substances was examined in a similar batch adsorption experiment for 0.05 mM mixed-metal solution in the presence of 1 mg L^{-1} of CBZ or humic acid. The pH of all solutions was maintained at 4, with the addition of NaOH if needed. 0.5 mL aliquots were taken at several time points over 200 h. Aliquots were immediately centrifuged for 10 min (15 000*g*), and the supernatant was diluted with eluent solution (0.5% HCl and 2% HNO_3) prior to quantification. Au adsorption isotherm experiments were performed at initial concentrations between 0.005 and 2.5 mM. Aliquots were sampled after reaching equilibrium (200 h) and treated in the same manner as samples from kinetic experiments.

2.3 Synthesis and adsorption test of mucin nanofibers

PGM (30 mg) was added to a PCL solution (10%) in acetic acid and mixed using a magnetic stirrer. The solution was loaded into a lab-built electrospinning setup. The solution was introduced into a plastic syringe and vertically ejected at a constant flow rate (MRC microinjection pump, 300 nL min^{-1}) through a 22G blunt needle connected to a high-voltage power supply (Bertan, series 230). A grounded metallic rectangular collector plate 25 cm from the needle tip was used as the nanofiber (NF) collector. The electrospinning was performed in a closed chamber under controlled temperature (25 °C) and 70% relative humidity. The synthesized NFs were collected for 5 hours and then removed from the collector as a single mat fabric. Adsorption experiments with NF mats were conducted by placing a piece of the mucin-based mat (0.75 mg, 0.5 × 0.5 cm) in 50 mL of 0.05 mM mixed-metal solution. The reversible metal desorption potential was examined by immersing a mixed-metal-loaded NF membrane for 48 hours in 2 mL of 0.1 M EDTA, followed by washing in deionized (DI) water and drying overnight in a desiccator.

2.4 Catalytic oxidation experiments for BPA degradation

For the PMS activation experiments, Au@mucin NPs were synthesized using three times more Au than in the selectivity experiments. The amount of mucin was also tripled, and the solution was heated to 70 °C to expedite the reaction. The kinetic catalytic experiments were conducted in glass vials while mixing 0.015 g L^{-1} of Au NPs used as the catalyst, 1 mg L^{-1} BPA used as the model pollutant, 0.2 mM of PMS as the oxidant, and 1 mM sodium bicarbonate as a solution buffer. The experiments were performed in duplicates for five hours under controlled conditions (25 °C and mixing at 300 rpm). Aliquots (100 μL, diluted ×4 with DI) were taken periodically and centrifuged (18 000*g* for 10 min) to separate the Au NPs from the supernatant. Then, 200 μL of supernatant was diluted ×2 with DI, transferred to 2 mL glass HPLC vials, and stored in the refrigerator before BPA analysis. A control experiment was performed without the addition of Au NPs. To investigate the adsorption of BPA by Au NPs (instead of decomposition), the same experimental solution was prepared, but without the addition of PMS. To examine the catalysis mechanism, 0.1 M of methanol (MeOH) was added as a radical scavenger to the basic mixture (PMS + BPA + Au NPs). The pH effect on the catalytic process was examined by altering the pH at the range of 2 to 10 using HCl or NaOH. To test the selectivity of the PMS activation, the catalytic reaction was also performed with *p*CBA instead of BPA, maintaining the same initial conditions. The catalytic performance of the Au@mucin NFs was conducted in the same manner, but instead of using Au NPs in dispersion, a piece of Au NF mat was added to the solution to reach the same concentration of Au NPs as in the original reaction. The NF mat was examined for 4 cycles with the same initial BPA concentration (between each cycle, the Au@mucin NF composite was washed with DI and dried). In these experiments, aliquots were not centrifuged prior to HPLC measurements.

2.5 Characterization methods

X-ray photoelectron spectroscopy (XPS) spectra were measured in ESCALAB QXi (Thermo Scientific, USA) to assess the oxidation state of the adsorbed metals in the mucin NFs. An Al Kα ($h\nu$ = 1486.6 eV) monochromatic source was used with a spot diameter of 900 μm. A pass energy of 40 eV was used for all high-resolution measurements. Charge compensation was conducted with an electron-ion dual beam. NF mats were tested at three different points to ensure homogeneity and a representative measurement was selected. The morphologies of the NPs and NFs were examined by an environmental scanning electron microscope (ESEM, Quanta 200 FEG) in high vacuum mode with an acceleration voltage of 20 kV. Sputtering of chromium was required prior to ESEM imaging for contrast enhancement. The sputtering (SPI sputter) was performed at 1.2 kV for 120 seconds. Au NPs formation was examined with a UV-visible spectrophotometer (Shimadzu 2600) in the 200–700 nm range.

X-ray diffraction (XRD) patterns for metal-mixture precipitates and NFs, were collected using a Bruker's D8 Discover diffractometer with the setup of Θ:Θ Bragg–Brentano geometry. The source used was a copper anode with an LYNXEYE XE linear detector. The diffraction patterns were collected between 20° and 60° 2Θ with step 0.02° 2Θ for 1 second per step. The analysis was obtained by comparing the diffracted beams of each material with a reference database in JCPDS (Joint Committee on Powder Diffraction Standards) library materials.

2.6 Quantification methods

All metal concentrations were determined by inductively coupled plasma mass spectroscopy (ICP-MS, 7800, Agilent, US). The removal of each metal was normalized to mucin mass (Q_e, mg g^{-1}) and was calculated using the follow equation:

$$Q_e = \frac{(C_i - C_e)V}{m} \quad (1)$$

where C_i and C_e (mg L^{-1}) are the initial and equilibrium concentrations of the metal, respectively; V is the volume of solution in the experiment (mL), and m is the total adsorbent mass (mg).

BPA and *p*CBA concentrations were quantified using high-performance liquid chromatography (HPLC, Agilent 1260 Infinity Series) coupled with a photodiode array UV-vis detector. A sample volume of 100 μL was injected into a Fast-guard Poroshell 120 (4.6 mm, 5 μm) pre-column and Poroshell 120 EC C18 (250 mm × 4.6 mm, 4 μm) column (Agilent Technologies, USA) at 30 °C. The mobile phase was an isocratic mixture comprising 70% HPLC-grade acetonitrile (Bio-Lab Ltd, Israel) and 30% DI water with 1% phosphoric acid (Merck KGaA, Germany) at a flow rate of 0.6 mL min^{-1}. BPA was detected at a retention time of 5.25 min with an absorption wavelength of 200 nm. *p*CBA was detected at a retention time of 5.25 min with an absorption wavelength of 234 nm (mobile phase MeOH : DI water with 1% acetic acid (55 : 45/v : v)).

3. Results and discussion

3.1 Selective adsorption from the metal mixture and gold nanoparticle formation

The adsorption of metals from a mixed solution of five metals used as a wastewater model solution, was examined. The binding strength of each metal cation to mucin depends on the metal's valency, the hydrolytic nature of the metal in the given solution pH, and the structure and binding site of the mucin molecule.[47] Small cations with low valency bind weakly to mucin and thus can detach quickly, unlike cations with high valency. Furthermore, based on the soft–hard acid–base theory, it can be concluded that soft acids such as Hg and Pd will preferably bind covalently to sulfated groups in mucin, which are considered hard bases. However, hard metals (*e.g.*, Al^{3+} and Fe^{3+}) expected to bind electrostatically to carboxylate groups.[33] Thus, for the metals in this study, it was expected that Au^{3+} would strongly attach to mucin, followed in decreasing order of affinity by Al^{3+}, Pd^{2+}, and Cu^{2+} and Fe^{2+}.

Fig. 1A shows the difference between adsorption rates at the steady state for each metal when in combination (mixed), compared to their adsorption from a solution when isolated (*i.e.*, no competition with other metals). When isolated in solution, Au exhibited the highest adsorption out of the metals due to its strong affinity to mucin as a trivalent large cation. Also, as was demonstrated in our previous research regarding mercury–mucin interactions,[23] there could be several binding sites in mucin that can bind soft acids such as Au, including carboxylate, sulfate, and amide. Al also exhibited large adsorption as a trivalent hydrolytic cation that can bind electrostatically to carboxylate groups.[33] Pd^{2+} exhibited high adsorption, although expected to bind less strongly to mucin as a divalent cation. We suggest that the high adsorption levels of Pd^{2+} is attributed to its function as a soft acid, which attaches strongly to the cysteine-rich domain in mucin (to the thiol group).[48] Cu^{2+} and Fe^{2+}, on the other hand, obtained poor adsorption to mucin as intermediate acids, which reversibly bind to mucin sites in equilibrium and thus can keep moving freely in the solution.

However, the adsorption trends in the mixed-metal solution change significantly compared to those in the isolated-metal solutions. First, the overall metal adsorption in the mixed solution was higher than the sum of the metals adsorbed across each isolated-metal solution experiment. This can be explained by the higher starting ion concentration in the mixed-metal solution (in the mixed solution, there are 5 times more ions than in the isolated-metal solutions), which drives higher adsorption rates and equilibrium levels. Interestingly, Fe adsorption in the mixed

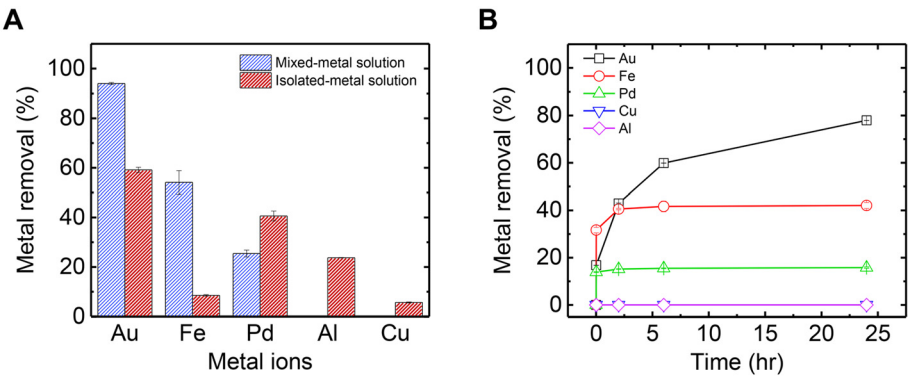

Fig. 1 (A) Metal removal by mucin from mixed-metal and isolated-metal aqueous solutions (initial concentration of each metal: 0.05 mM in steady state). (B) Removal of all metals by mucin as a function of time from an aqueous mixed-metal solution containing 0.05 mM of each metal. All experiments were conducted in 0.1 g L^{-1} dissolved mucin and solution pH of 4. Error bars represent one standard deviation from an average of two measurements.

solution was almost 5 times more than the levels adsorbed compared to the pristine Fe solution. It can be assumed that in the mixed solution, some of the Fe^{2+} ions were oxidized to Fe^{3+} by one of the other metals in the mixture (with higher reduction potential). Because Fe^{3+} can bind more strongly to mucin than Fe^{2+} in the sole solution (Fig. S1†), Fe adsorption was higher in the mixed solution than in the isolated solution. In addition, Fe^{3+} is kinetically more active than Al^{3+}, and has a greater affinity to mucin than other trivalent metals, as shown in previous studies concerning mucin's role in adsorbing metals in rats and humans.[33,47,49] Thus, Fe could occupy the mucin's binding sites faster, at the expense of Al^{3+} and Pd^{2+} adsorption. Third, although Au has the slowest kinetics in the mixture (Fig. 1B), it did reach the highest adsorption in equilibrium in isolated- and mixed-metal solutions (Fig. S2† shows the kinetics in the mixture until it reaches a steady state). As shown in Fig. 1B, in the first few minutes, Fe reached a higher level of removal than Au, but this trend eventually reversed. Furthermore, there is a substantial increase in Au adsorption in the mixed-metal solution, reaching almost complete removal of Au ions from the solution. To explain these observations, a deeper examination of Au's interactions with mucin is examined in the next section.

3.2 Gold adsorption and recovery by mucin

Fig. 2A shows the Au adsorption kinetics by mucin across three different Au concentrations (as a sole metal), which were fit to a pseudo-second-order model (Table S1† summarizes the kinetic values). It is evident that lower concentrations are associated with faster kinetics: in 0.025 mM solution, a steady state was reached after 24 h, with a kinetic rate of 0.0019 g mg^{-1} h^{-1}, while the adsorption kinetics in the 0.05 mM solution was quite low (k = 3.21 × 10^{-4} g mg^{-1} h^{-1}), reaching equilibrium after 200 h. The 0.1 mM solution did not reach a plateau in this time frame (k = 7.57 × 10^{-5} g mg^{-1} h^{-1}). In a previous study, such slow adsorption kinetics was not observed for mercury—another soft acid of similar adsorptive properties—which suggests that heavy ions' attachment to mucin in a solution could occur within the first seconds.[50] The relatively slow kinetics of Au, which was also observed in the mixed-metal solution (Fig. 1B), can be attributed to the co-occurrence of Au reduction during adsorption. The first visual evidence of the Au chemical reduction was the change in the solution color from light yellow to light red. The transparent red hue is the typical color of suspended Au NPs in a solution, contributing to the visible-light adsorption due to the surface plasmon resonance of the particles.[23,51,52] The Au adsorption isotherm (Fig. 2B) suggests a maximum Au capacity of 750 mg g^{-1} on mucin. This value is consistent with and even higher than similar Au recovery methods explored in previous studies using different biomaterials.[20,53,54]

Fig. 2C compares the decrease of Au ions from the solution and the increase of Au NPs concentration (see Fig. S3† for UV-vis absorbance spectra of the NPs). In the first few hours, though fewer Au ions were removed from the solution to be treated, no Au NPs were detected, indicating that only adsorption occurred in these hours. It can be assumed that Au ions are first attached to thiol groups in the cysteine-rich domains in mucin. The thiol group can interact with gold by a coordination-type bond through the sulfur lone-pair electron. When deprotonated, this group binds covalently to gold, creating an RS–Au bond (where R represents organic moiety) with a strength close to that of gold–gold bond.[55] This interaction can induce the reduction of gold ions, forming the initial Au NP seeds.[56,57] As time progresses, more Au ions are reduced and attached to the existing nucleation sites, allowing the NPs to grow.[58,59] This mechanism can also explain the slow kinetics of the overall Au removal process that was observed compared to the other metals (Fig. 1B). It should be noted that the NPs formation kinetics could be expedited (to 2–3 hours) by heating the solution to 70 °C, as was established in a previous paper.[35]

It was observed that the mixed-metal solution, after a few hours from the addition of mucin, changed in color from light yellow to light red, similar to the solution with Au in

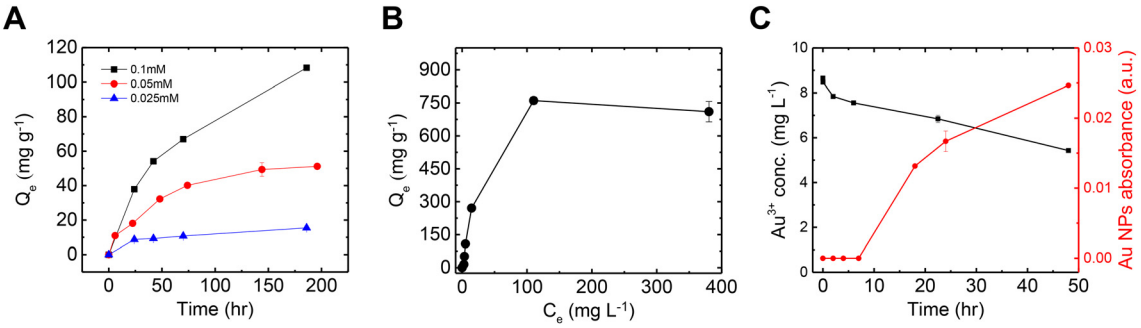

Fig. 2 Au recovery performance by mucin. (A) Removal of Au^{3+} by mucin as a function of time from aqueous solutions containing 0.025 mM, 0.05 mM and 0.1 mM Au^{3+}. (B) Adsorption isotherm illustrating equilibrium removal levels of Au^{3+} by mucin across a range of concentrations between 0.005 and 2.5 mM Au^{3+}. (C) Au^{3+} concentration measured in inductively coupled plasma *vs.* Au nanoparticles concentration measured in UV-vis during the first 48 h in a 0.05 mM solution. All experiments were conducted in 0.1 g L^{-1} dissolved mucin and at a solution pH of 4. Error bars represent one standard deviation from an average of two measurements.

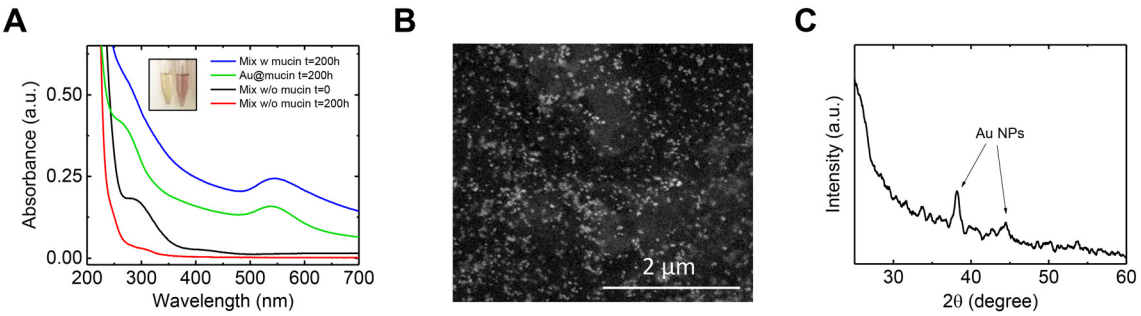

Fig. 3 Au nanoparticle (NP) formation in the mixed-metal solution. (A) UV-vis absorption of Au nanoparticles in the mixed-metal solution both with and without the presence of mucin. Inset: Optical image of mixed-metal solution before (left) and after (right) the addition of mucin. (B) Scanning electron microscope (SEM) image of Au nanoparticles formed in the mixed-metal solution in the presence of mucin. (C) X-ray diffraction (XRD) pattern of the mixed-metal precipitate after centrifugation.

isolation. This observation again indicates the formation of Au NPs with mucin's assistance. The UV-vis spectra of the mixed-metal solution were compared to that of the Au solution, both with the addition of mucin (Fig. 3A). A distinctive peak of Au NPs at ~540 nm was observed in both solutions 200 h after exposure to mucin. The Au NP plasmonic peak showed a red shift in the mixed-metal solution compared to the pristine Au solution (545 nm *vs.* 538 nm), possibly due to larger NPs forming in the mixed-metal solution. A comparison of SEM images of the NPs from the mixed-metal solution (Fig. 3B) and Au NPs in the isolated solution (Fig. S4†) confirms that the Au NPs in the mixed-metal solution were indeed larger than those in the isolated solution (20.3 ± 4.6 nm compared to 13.5 ± 4.0 nm). The larger NPs in the mixed solution suggest that more Au ions were reduced to atoms and attached together, which is consistent with the higher removal of Au in the mixed solution than in the solution with isolated Au (Fig. 1A).

The reasoning behind the elevated reduction of Au ions in the mixed-metal solution compared to Au in isolation can be found by comparing the Au UV-vis spectra to that obtained in the absence of mucin (Fig. 3A). In such a solution (red curve), no plasmonic peak of Au was measured, indicating that Au NPs were not formed without mucin. Furthermore, in the control solution (*i.e.*, a mixed-metal solution without mucin), two peaks at ~300 nm and ~400 nm were initially observed and were nearly non-existent after 200 h of shaking. These peaks correspond to Fe^{2+} and Pd^{2+}, respectively, and their decrease can be explained by a potentially galvanic reaction for these ions with other metals in the mixture. It should be noted that even if Au ions were taking part of the redox and reduced by Pd or Fe, it is evident that they did not cause the transformation into NPs without mucin. Mucin is also known not only as a reducing agent but also as a stabilizer and a capping one, and it even has a role in determining the shape and size of NPs.[35,37] Overall, it could be assumed that in the mixture, Pd or Fe were responsible for a portion of the Au ions' reduction over time in addition to the ions reduced by mucin. However, mucin is responsible for the NPs formation and growth on top of the existing seeds.

The crystalline nature of the Au NPs was evaluated using X-ray diffraction (XRD, Fig. 3C). The spectra revealed the distinctive peaks of the FCC Au NPs (38.2° and 44.5°, corresponding to (111) and (200) planes according to JCPDS file no. 04-0784). No other significant peaks that could be related to Pd or Fe were observed, implying no formation of any other crystalline form.

The effect of small common ions such as K^+, Na^+, and Ca^{2+} on the Au recovery by mucin, was also evaluated. Fig. S5A† shows that the appearance of such cations in solution did not change the Au NP formation. This stands in line with previous reports, in which small cations were only weakly bound to mucin and allowed mercury adsorption.[23] In addition, the influence of organic substances (such as CBZ or humic acid which may co-present in wastewater) was also examined. The mixed-metal solution selectivity was verified through the formation of Au NPs in such complex media (UV-vis spectra in Fig. S5B†).

Generally, the exclusive reduction of Au ions (compared to other metals in the experiments) by mucin can be explained by two conditions that uniquely co-exist for Au: (1) the binding extent and affinity of the Au cation to mucin compared to that of the other metals and (2) the reduction potential of Au relative to that of mucin compared to that of the other metals. For the reduction of an ion to occur, its reduction potential should be higher than the oxidizing agent. In this case, mucin's reduction sites have an assumed standard reduction potential of −0.318 eV,[28] whereas the reduction potential of Au is 1.498 eV. So not only does Au have the highest potential to be reduced by mucin (Table S2† outlines the reduction potential of each metal), but it also has the highest adsorption to mucin (both in isolation and in the mixed-metal solutions), which exacerbates its tendency to be reduced as compared to the other metals examined.[60] One would expect Pd to also transform into NPs (due to its elevated reduction potential); however, no Pd NPs were formed in the mixed or isolated solutions. As seen from previous studies, it lacks the conditions for Pd to be reduced spontaneously in a bio-assisted synthesis by a biomaterial (most studies were not performed in ambient conditions and required neutral pH or heat).[61–64]

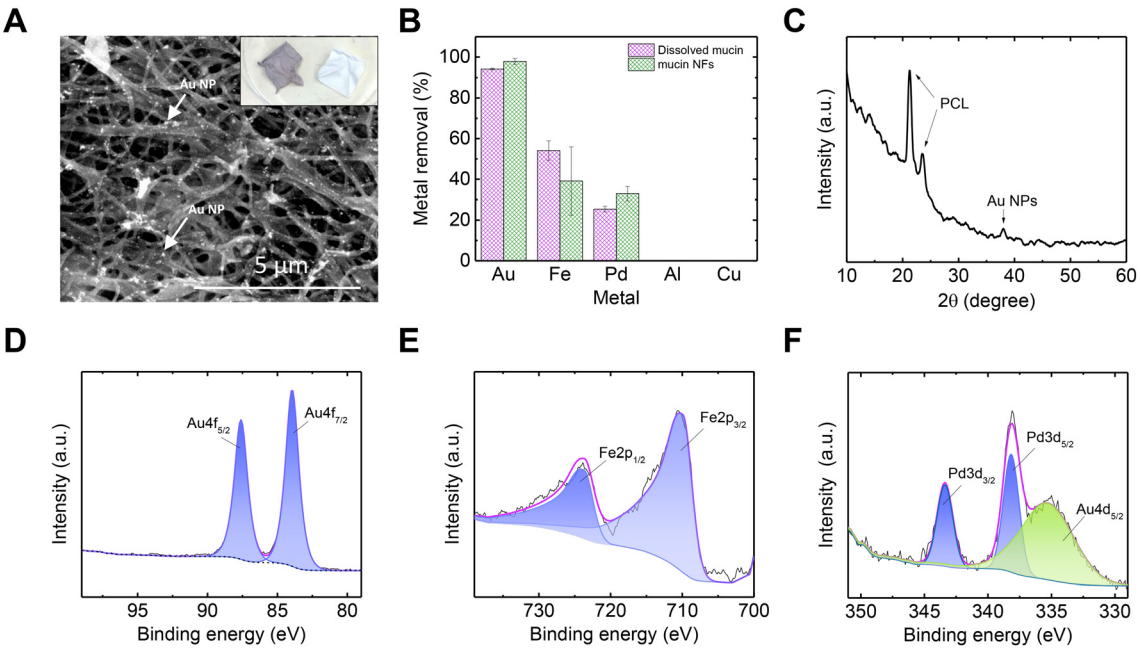

Fig. 4 Metal extraction with mucin in a nanofiber (NF) form. (A) Scanning electron microscope image of Au nanoparticles formed in the mixed-metal aqueous solution in the presence of mucin/PCL NFs. Inset is an optical image of the pristine fibers (right) and the fibers embedded with Au nanoparticles (left). (B) Metal removal by mucin dissolved in solution and as nanofibers from a mixed-metal solution. (C) X-ray diffraction pattern of the nanofibers. (D)–(F) Representative X-ray photoelectron spectroscopy spectra of (D) Au 4f (E) Fe 2p (E) Pd 3d. Error bars in (B) represent one standard deviation from an average of two measurements.

3.3 Practical application of mucin for gold recovery

After establishing an understanding of the mechanism behind mucin's ability to recover Au exclusively from a mixed-metal solution, we suggest a practical form of using mucin as an adsorbent and reductive treatment agent for metal-rich wastewater.[65] Using an electrospinning technique, mucin-based NFs were produced, composed of PGM (pig gastric mucin) and PCL (polycaprolactone). A SEMimage of the NFs after the adsorption process is shown in Fig. 4A (for SEM image of pristine mucin/PCL NFs, see Fig. S6†). Once mucin is formed into a NF mat, such a macro-scaled, solid form can allow facile handling compared to dissolved mucin.

Though the overall trend in metal removal from the mixed-metal solution was similar for the NF mucin and the dissolved mucin (Fig. 4B), the amount of Au adsorbed was higher for the NFs than the suspended mucin (207.91 *vs.* 84.45 mg g^{-1}, respectively). This can be attributed to the fact that water acidity causes more mucin glycoprotein aggregation and precipitation,[25] a phenomenon suppressed if the mucin is incorporated within a non-dissolving solid structure such as a NF. This aggregation prevention is another advantage of using mucin in a NF form, which allows the exposure of more binding sites for the Au ions. This elevated performance of mucin in the NF architecture has also been demonstrated in mercuric adsorption, in which higher rates of mercury ions were adsorbed to the mucin-impregnated NF than to dissolved mucin.[23] The XRD spectrum of the Au NPs in the NF is shown in Fig. 4C. The distinctive peak of Au NPs (38.2° corresponding to (111) planes according to JCPDS file no. 04-0784) is accompanied by two peaks at 21.3 and 23.5 attributed to crystalline PCL.

Next, the NF mat was investigated by XPS to understand better the adsorbed metals' oxidation states (Fig. 4D–F). The Au 4f binding energies were 84.1 eV and 87.8 eV, corresponding to $4f_{7/2}$ and $4f_{5/2}$ in the Au^0 oxidation state, respectively. No peaks corresponding to Au^{3+} were observed, supporting a complete NP formation (with a metallic oxidation state of Au^0). The peaks at 724.2 eV and 710.4 eV correlate to Fe $2p_{1/2}$ and Fe $2p_{3/2}$, respectively, and could be fitted to both Fe^{2+} and Fe^{3+}. The Fe oxidation observed during experiments can again be explained by a galvanic reaction with other metal in the mixture with higher reduction potential (see reduction potential of Au and Pd in Table S2†). The Pd 3d binding energies were 343.4 eV and 338.2 eV, attributed to the Pd $3d_{3/2}$ and $3d_{5/2}$, respectively. These values were fitted best to $PdCl_2$,[66] which could participate in the mucin molecule after Pd^{2+} was adsorbed. No peaks relating to Al or Cu were observed in the spectra (Fig. S7†), which is consistent with the ICP measurements of the metal removal (Fig. 1A).

To achieve a pristine Au@mucin NF membrane (*i.e.*, membrane that does not contain non-Au metal ions), the NF mat was cleaned with 0.1 M EDTA. EDTA was used due to its property as a chelate and its ability to capture only ions while leaving the Au NPs unharmed. Indeed, an ICP measurement of the solution after 24 h, revealed a release of almost all the Fe and most of the Pd, while only a negligible amount of Au

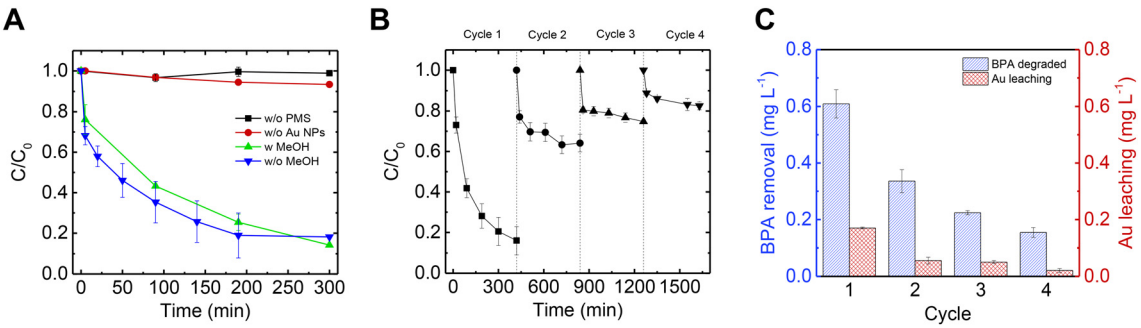

Fig. 5 Peroxymonosulfate (PMS) activation for bisphenol A (BPA) degradation. (A) Removal of BPA with PMS and Au nanoparticles in dispersion. $[BPA]_0$ = 1 mg L^{-1}; $[PMS]_0$ = 0.2 mM; $[Au\ NPs]_0$ = 0.015 g L^{-1}. (B) Removal of BPA with Au nanoparticle-embedded mucin nanofibers (in the presence of PMS) over four cycles. (C) BPA removal by Au-embedded nanofibers (blue) and Au leaching (red) for each cycle in (B).

was present in the desorbing solution. The associated atomic concentrations (calculated with XPS) of all elements before and after cleaning are shown in Tables S3 and S4,† respectively; no Pd or Fe after cleaning were detected.

3.4 Bisphenol A degradation using recovered Au nanoparticles catalysts and PMS

Following removal of non-Au metal ions by EDTA, the Au@mucin NF composite was used for a subsequent catalysis process. First, the catalytic oxidation reaction was examined using suspended Au NPs as a catalyst for the decomposition of BPA with the addition of PMS. Fig. 5A shows the decomposition of BPA during the catalytic process. When using noble metal NPs, the activation mechanism of PMS is known to be electron mediation transfer.[42,43] To validate this non-radical mechanism route in which noble metal NPs are used, a radical scavenger, MeOH, was added in excess to the reaction and the decomposition rate of BPA was tested and compared. As shown in Fig. 5A, the decomposition of BPA occurred and lasted 5 hours (blue curve). With the addition of MeOH no significant change in the reaction rate was observed (green curve), indicating that radicals were not responsible for the BPA oxidation. In addition, the same reaction was conducted without the presence of PMS (black curve) to rule out adsorption of the BPA by the Au@mucin; in this latter case no significant decrease of BPA was shown. Furthermore, although PMS is a strong oxidizer, with a redox potential of 1.82 V, it has been shown to react directly with organic contaminants with a low reaction rate.[40] As shown in the control experiment (*i.e.*, without the presence of the catalyst, but only with PMS and BPA), only a slight decrease in the BPA concentration was detected in the experiment timeframe (red curve). Further on, to test the stability of the catalyst, the PMS activation was performed at different solution pH values (Fig. S8†). The results indicate that until reaching pH 7, the performance was nearly unharmed. This limited pH effect at acidic conditions support the assumption of non-radical pathway (as radicals can be scavenged by excess H^+ in some radical-based catalytic systems).[67,68] Alkaline pH, however, resulted in a drastic decrease in the BPA degradation which might be related to the hydrolysis of PMS,[69] or to the increase in anionic BPA species (pK_a = 9.6).[70]

PMS activation through electron-mediated transfer is more pronounced for phenolic compounds, as was established in previuos studies.[42,43,68] The catalytic experiment was conducted in the presence of 4-chlorobenzoic acid (*p*CBA), a non-phenolic molecule commonly used as an indicator for radical formation (as it reacts quickly with both OH· and $SO_4\cdot^-$).[71,72] Not surprisingly, *p*CBA was not degraded in the PMS-activation reaction, highlighting the dominancy of the non-radical degradation pathway and selectivity towards phenolic compounds.

After establishing the electron mediation transfer reaction mechanism, it was possible to run the same reaction with Au embedded in NFs, due to the assumption that the PMS activation is not driven by radicals and other organic matter in the solution could thus stay intact. Furthermore, in the case of using the catalyst embedded in fibers and not in dispersion, their separation is much easier, and recyclability is possible. Hence, the NFs were examined for 4 cycles and BPA concentration was measured across time for each cycle as depicted in Fig. 5B. In the first cycle, the performance of the membrane was similar to when NPs were used in suspension, but it took a bit longer to reach a steady state (7 h *vs.* 5 h). Although the performance of the membrane decreased between each cycle, BPA was still degraded each cycle. The decrease in catalytic efficiency between each cycle can be explained by the accumulation of oxidation products of BPA on the surface of the Au NPs.[43,68] Across all four cycles, the amount of BPA decomposed was 1.32 mg L^{-1} (sum of the BPA degradation column heights in Fig. 5C). In addition, the Au leaching from the membrane was measured after each cycle as shown in Fig. 5C, and totaled 0.3 mg L^{-1} (sum of the Au leaching column heights in Fig. 5C) which is less than 2% of the original Au in the NF.

3.5 From metal wastewater to organic waste removal

Au concentrations in industrial wastewater can range from a few ppb to dozens of ppm.[23,73] In the spirit of circular

economy, the entire exploitation of mucin in the whole process was calculated. In this study, 1 g of mucin, could transform 750 mg of Au into NPs, allowing a secondary use of this precious metal from wastewater, which otherwise would have been thrown away with other less expensive metals. The recovered Au NPs could then also assist in eliminating additional waste—this time an organic one—in a highly selective reaction: PMS activation for the oxidation of the pollutant BPA. From the same 1 g of mucin, 50 mg of BPA could be decomposed. If taking into account the embedded Au@mucin in NFs, which could be used for several catalytic cycles, an even larger amount of BPA could be degraded.

1 g of mucin from the source that was used in this research (porcine stomach), costs ~$2.50 (CAS 84082-64-4). Another alternative is to use mucin extracted from jellyfish biomass.[29,74] It has been previously shown that jellyfish mucin can be embedded in NFs and form Au NPs.[37] In addition, the utilization of jellyfish is acceptable given the overpopulation of jellyfish causing enormous economic and environmental global damages.[75] If using jellyfish as the mucin source, the cost per 1 g of mucin would be substantially reduced to $0.002.

Further research might explore optimizing the economic circuit, focusing on the separation of other precious metals in solution. For instance, Pd, a highly desired metal used in various catalytic reactions, was shown to be more efficient than Au NPs for activating PMS.[43] If prioritizing Pd recovery, the separation of the metals could be accomplished in two steps: after recovering the Au, the remaining supernatant, containing Pd ions among other ions, could be heated to obtain conditions required for Pd reduction by mucin.

4. Conclusion

This study examined the unique and natural ability of the glycoprotein mucin, to selectively adsorb and recover specific metals. From a model wastewater mixed-metal solution containing Au, Pd, Cu, Fe, and Al ions, Au was favorably adsorbed by mucin over the other metals. This was shown both in the mixed-metal and isolated-metal solutions. Not only could mucin adsorb Au in a maximum capacity of 750 mg g^{-1}, but it also could reduce Au ions into Au NPs. This phenomenon occurred both in the mixed-metal and isolated-metal solutions. To allow a more practical use of mucin, mucin was embedded in NFs, and again tested for the adsorption of the metal mixture. The results were similar to those obtained with dissolved mucin. The retrieved NFs embedded with Au NPs could then be used to activate PMS for the oxidation of BPA. The activation mechanism with Au NPs was not based on radical-formation, and thus has the potential to be more selective in the decomposition of organic molecules. The Au NF mat was tested for BPA degradation over 4 cycles, and exhibited BPA degradation in each cycle with minimal associated Au leaching.

Overall, we demonstrated a two-step green treatment for wastewater that highly supports the nano circular economy framework: first, the use of a renewable natural resource (mucin) for selective recovery of Au from wastewater, without using any synthetic or harmful material for the reduction; second, the use of these recovered metals for a secondary decontamination through the degradation of toxic organic substance in highly selective catalysis. These processes avoid waste and pollution, keep products and materials in use as long as possible, and regenerate natural systems, showcasing this overall design as a prime example of the nano circular economy framework. Future studies may focus on quantifying the environmental impact, including the retention and the stability of gold NPs in mucin template, long-term operation, and compare the life cycle assessment (LCA) of this process against traditional decontaminating methods.

Conflicts of interest

No conflict of interest exists in the submission of this manuscript and the manuscript was approved by all authors for publication.

Acknowledgements

This research is supported by the Adams Fellowships Program of the Israel Academy of Sciences and Humanities. The authors would like to thank the Buchmann Scholarships Fund for its financial support. The authors would like to thank ADAMA Center for Novel Delivery Systems for providing support with the ICP-MS analytical measurements. The authors also acknowledge Dr. Pini Shekter for XPS analysis at the Wolfson Applied Materials Research Center, Tel-Aviv University. Lastly, the authors would like to thank Keren Hadar and Yulia Molotski for their help during the research. The graphical abstract was created using BioRender.

References

1 J. Ahmed, A. Thakur and A. Goyal, in *Biological Treatment of Industrial Wastewater*, ed. M. P. Shah, The Royal Society of Chemistry, 2021.
2 H. Umeda, A. Sasaki, K. Takahashi, K. Haga, Y. Takasaki and A. Shibayama, Recovery and Concentration of Precious Metals from Strong Acidic Wastewater, *Mater. Trans.*, 2011, **52**, 1462–1470.
3 A. Taghvaie Nakhjiri, H. Sanaeepur, A. Ebadi Amooghin and M. M. A. Shirazi, Recovery of precious metals from industrial wastewater towards resource recovery and environmental sustainability: A critical review, *Desalination*, 2022, **527**, 115510.
4 O. Abdi and M. Kazemi, A review study of biosorption of heavy metals and comparison between different biosorbents, *J. Mater. Environ. Sci.*, 2015, **6**, 1386–1399.
5 R. Singh, N. Gautam, A. Mishra and R. Gupta, Heavy metals and living systems: An overview, *Indian J. Pharmacol.*, 2011, **43**, 246–253.

6 X. Xu, Y. Yang, X. Zhao, H. Zhao, Y. Lu, C. Jiang, D. Shao and J. Shi, Recovery of gold from electronic wastewater by Phomopsis sp. XP-8 and its potential application in the degradation of toxic dyes, *Bioresour. Technol.*, 2019, **288**, 121610.
7 M. Moyo, G. Nyamhere, E. Sebata and U. Guyo, Kinetic and equilibrium modelling of lead sorption from aqueous solution by activated carbon from goat dung, *Desalin. Water Treat.*, 2016, **57**, 765–775.
8 J. Cao, Z. Xu, Y. Chen, S. Li, Y. Jiang, L. Bai, H. Yu, H. Li and Z. Bian, Tailoring the Asymmetric Structure of NH2-UiO-66 Metal-Organic Frameworks for Light-promoted Selective and Efficient Gold Extraction and Separation, *Angew. Chem., Int. Ed.*, 2023, **62**, e202302202.
9 S. Krishnan, N. S. Zulkapli, H. Kamyab, S. M. Taib, M. F. B. M. Din, Z. A. Majid, S. Chaiprapat, I. Kenzo, Y. Ichikawa, M. Nasrullah, S. Chelliapan and N. Othman, Current technologies for recovery of metals from industrial wastes: An overview, *Environ. Technol. Innovation*, 2021, **22**, 101525.
10 F. Burat, H. Baştürkcü and M. Özer, Gold&silver recovery from jewelry waste with combination of physical and physicochemical methods, *Waste Manage.*, 2019, **89**, 10–20.
11 Y. Chen, M. Xu, J. Wen, Y. Wan, Q. Zhao, X. Cao, Y. Ding, Z. L. Wang, H. Li and Z. Bian, Selective recovery of precious metals through photocatalysis, *Nat. Sustain.*, 2021, **4**, 618–626.
12 A. Golnaraghi Ghomi, N. Asasian-Kolur, S. Sharifian and A. Golnaraghi, Biosorpion for sustainable recovery of precious metals from wastewater, *J. Environ. Chem. Eng.*, 2020, **8**, 103996.
13 F. Xie, T. A. Zhang, D. Dreisinger and F. Doyle, A critical review on solvent extraction of rare earths from aqueous solutions, *Miner. Eng.*, 2014, **56**, 10–28.
14 N. Das, Recovery of precious metals through biosorption — A review, *Hydrometallurgy*, 2010, **103**, 180–189.
15 F. Veglio' and F. Beolchini, Removal of metals by biosorption: a review, *Hydrometallurgy*, 1997, **44**, 301–316.
16 S. W. Al Rmalli, A. A. Dahmani, M. M. Abuein and A. A. Gleza, Biosorption of mercury from aqueous solutions by powdered leaves of castor tree (Ricinus communis L.), *J. Hazard. Mater.*, 2008, **152**, 955–959.
17 S. Srivastava and P. Goyal, *Novel biomaterials: decontamination of toxic metals from wastewater*, Springer Science & Business Media, 2010.
18 J. Aburabie, S. Mohammed, A. Kumaran and R. Hashaikeh, From waste to wealth: chelating polymeric membranes for precious palladium recovery from wastewater, *J. Mater. Chem. A*, 2023, **11**, 22845–22858.
19 M. M. H. Rocky, I. M. M. Rahman, F. B. Biswas, S. Rahman, M. Endo, K. H. Wong, A. S. Mashio and H. Hasegawa, Cellulose-based materials for scavenging toxic and precious metals from water and wastewater: A review, *Chem. Eng. J.*, 2023, **472**, 144677.
20 X. Gao, Y. Zhang and Y. Zhao, Biosorption and reduction of Au (III) to gold nanoparticles by thiourea modified alginate, *Carbohydr. Polym.*, 2017, **159**, 108–115.
21 C. Mack, B. Wilhelmi, J. R. Duncan and J. E. Burgess, Biosorption of precious metals, *Biotechnol. Adv.*, 2007, **25**, 264–271.
22 R. Nudelman, E. Gloukhikh, A. Rekun and S. Richter, Investigation of the pH-dependence of dye-doped protein–protein interactions, *Protein Sci.*, 2016, **25**, 1918–1923.
23 S. Gavriely, S. Richter and I. Zucker, Mucin-Based Composites for Efficient Mercuric Biosorption, *Adv. Sustainable Syst.*, 2022, **6**, 2200081.
24 N. Hendler, B. Belgorodsky, E. D. Mentovich, M. Gozin and S. Richter, Efficient Separation of Dyes by Mucin: Toward Bioinspired White-Luminescent Devices, *Adv. Mater.*, 2011, **23**, 4261–4264.
25 R. Bansil and B. S. Turner, Mucin structure, aggregation, physiological functions and biomedical applications, *Curr. Opin. Colloid Interface Sci.*, 2006, **11**, 164–170.
26 C. E. Wagner, K. M. Wheeler and K. Ribbeck, Mucins and Their Role in Shaping the Functions of Mucus Barriers, *Annu. Rev. Cell Dev. Biol.*, 2018, **34**, 189–215.
27 R. A. Cone, Barrier properties of mucus, *Adv. Drug Delivery Rev.*, 2009, **61**, 75–85.
28 R. Nudelman, H. Alhmoud, B. Delalat, S. Fleicher, E. Fine, T. Guliakhmedova, R. Elnathan, A. Nyska, N. H. Voelcker, M. Gozin and S. Richter, Jellyfish-Based Smart Wound Dressing Devices Containing In Situ Synthesized Antibacterial Nanoparticles, *Adv. Funct. Mater.*, 2019, **29**, 1902783.
29 L. R. Steinberger, T. Gulakhmedova, Z. Barkay, M. Gozin and S. Richter, Jellyfish-Based Plastic, *Adv. Sustainable Syst.*, 2019, **3**, 1900016.
30 A. Masuda, T. Baba, N. Dohmae, M. Yamamura, H. Wada and K. Ushida, Mucin (Qniumucin), a Glycoprotein from Jellyfish, and Determination of Its Main Chain Structure, *J. Nat. Prod.*, 2007, **70**, 1089–1092.
31 G. Petrou and T. Crouzier, Mucins as multifunctional building blocks of biomaterials, *Biomater. Sci.*, 2018, **6**, 2282–2297.
32 P. Pärt and R. A. C. Lock, Diffusion of calcium, cadmium and mercury in a mucous solution from rainbow trout, *Comp. Biochem. Physiol., Part C: Pharmacol., Toxicol. Endocrinol.*, 1983, **76**, 259–263.
33 J. J. Powell, R. Jugdaohsingh and R. P. H. Thompson, The regulation of mineral absorption in the gastrointestinal tract, *Proc. Nutr. Soc.*, 1999, **58**, 147–153.
34 S. Gavriely, W. Hadibrata, R. Nudelman, K. Aydin and S. Richter, One-Pot Bio-Assisted Synthesis of Stable Ag–AgCl System Using Jellyfish-Based Scaffold for Plasmonic Photocatalysis Applications, *Adv. Sustainable Syst.*, 2021, **5**, 2100099.
35 R. Nudelman, H. Alhmoud, B. Delalat, I. Kaur, A. Vitkin, L. Bourgeois, I. Goldfarb, A. Cifuentes-Rius, N. H. Voelcker and S. Richter, From nanoparticles to crystals: one-pot programmable biosynthesis of photothermal gold structures and their use for biomedical applications, *J. Nanobiotechnol.*, 2022, **20**, 482.
36 N. Hendler, L. Fadeev, E. D. Mentovich, B. Belgorodsky, M. Gozin and S. Richter, Bio-inspired synthesis of chiral silver

nanoparticles in mucin glycoprotein—the natural choice, *Chem. Commun.*, 2011, **47**, 7419–7421.
37 R. Nudelman, S. Gavriely, D. Bychenko, M. Barzilay, T. Gulakhmedova, E. Gazit and S. Richter, Bio-assisted synthesis of bimetallic nanoparticles featuring antibacterial and photothermal properties for the removal of biofilms, *J. Nanobiotechnol.*, 2021, **19**, 1–10.
38 N. Joudeh and D. Linke, Nanoparticle classification, physicochemical properties, characterization, and applications: a comprehensive review for biologists, *J. Nanobiotechnol.*, 2022, **20**, 262.
39 M. J. Ndolomingo, N. Bingwa and R. Meijboom, Review of supported metal nanoparticles: synthesis methodologies, advantages and application as catalysts, *J. Mater. Sci.*, 2020, **55**, 6195–6241.
40 J. Wang and S. Wang, Activation of persulfate (PS) and peroxymonosulfate (PMS) and application for the degradation of emerging contaminants, *Chem. Eng. J.*, 2018, **334**, 1502–1517.
41 H. V. Lutze, S. Bircher, I. Rapp, N. Kerlin, R. Bakkour, M. Geisler, C. von Sonntag and T. C. Schmidt, Degradation of Chlorotriazine Pesticides by Sulfate Radicals and the Influence of Organic Matter, *Environ. Sci. Technol.*, 2015, **49**, 1673–1680.
42 Y.-Y. Ahn, H. Bae, H.-I. Kim, S.-H. Kim, J.-H. Kim, S.-G. Lee and J. Lee, Surface-loaded metal nanoparticles for peroxymonosulfate activation: Efficiency and mechanism reconnaissance, *Appl. Catal., B*, 2019, **241**, 561–569.
43 Y.-Y. Ahn, E.-T. Yun, J.-W. Seo, C. Lee, S. H. Kim, J.-H. Kim and J. Lee, Activation of Peroxymonosulfate by Surface-Loaded Noble Metal Nanoparticles for Oxidative Degradation of Organic Compounds, *Environ. Sci. Technol.*, 2016, **50**, 10187–10197.
44 G. Y. Kim, D. Lee, H.-S. Choe, J.-M. Park, S. Jeong, E. J. Park, J. W. Lee, C. Lee and J.-H. Kim, Yolk–shell-type gold nanosphere-encapsulated mesoporous silica for catalytic oxidation of organic pollutants in the presence of persulfate, *Environ. Sci.: Nano*, 2022, **9**, 2510–2520.
45 P. Halli, B. P. Wilson, T. Hailemariam, P. Latostenmaa, K. Yliniemi and M. Lundström, Electrochemical recovery of tellurium from metallurgical industrial waste, *J. Appl. Electrochem.*, 2020, **50**, 1–14.
46 Y. Rakhila, A. Elmchaouri, A. Mestari, S. Korili, M. Abouri and A. Gil, Adsorption recovery of Ag(I) and Au(III) from an electronics industry wastewater on a clay mineral composite, *Int. J. Miner., Metall. Mater.*, 2019, **26**, 673–680.
47 M. W. Whitehead, R. P. Thompson and J. J. Powell, Regulation of metal absorption in the gastrointestinal tract, *Gut*, 1996, **39**, 625–628.
48 K. Farhadi, M. Forough, A. Pourhossein and R. Molaei, Highly sensitive and selective colorimetric probe for determination of l-cysteine in aqueous media based on Ag/Pd bimetallic nanoparticles, *Sens. Actuators, B*, 2014, **202**, 993–1001.
49 M. E. Conrad, J. N. Umbreit and E. G. Moore, A role for Mucin in the absorption of inorganic iron and other metal cations: A study in rats, *Gastroenterology*, 1991, **100**, 129–136.
50 W. Li, B. Ju and S. Zhang, Preparation of cysteamine-modified cellulose nanocrystal adsorbent for removal of mercury ions from aqueous solutions, *Cellulose*, 2019, **26**, 4971–4985.
51 L. Zhang, K. Xia, Z. Lu, G. Li, J. Chen, Y. Deng, S. Li, F. Zhou and N. He, Efficient and Facile Synthesis of Gold Nanorods with Finely Tunable Plasmonic Peaks from Visible to Near-IR Range, *Chem. Mater.*, 2014, **26**, 1794–1798.
52 S. K. Ghosh and T. Pal, Interparticle Coupling Effect on the Surface Plasmon Resonance of Gold Nanoparticles: From Theory to Applications, *Chem. Rev.*, 2007, **107**, 4797–4862.
53 X. Chen, K. F. Lam, S. F. Mak and K. L. Yeung, Precious metal recovery by selective adsorption using biosorbents, *J. Hazard. Mater.*, 2011, **186**, 902–910.
54 Y.-C. Lo, C.-L. Cheng, Y.-L. Han, B.-Y. Chen and J.-S. Chang, Recovery of high-value metals from geothermal sites by biosorption and bioaccumulation, *Bioresour. Technol.*, 2014, **160**, 182–190.
55 H. Häkkinen, The gold–sulfur interface at the nanoscale, *Nat. Chem.*, 2012, **4**, 443–455.
56 J. Morales-Vidal, N. López and M. A. Ortuño, Chirality Transfer in Gold Nanoparticles by l-Cysteine Amino Acid: A First-Principles Study, *J. Phys. Chem. C*, 2019, **123**, 13758–13764.
57 I. Petean, G. H. Tomoaia, O. Horovitz, A. Mocanu and M. Tomoaia-Cotisel, Cysteine mediated assembly of gold nanoparticles, *J. Optoelectron. Adv. Mater.*, 2008, **10**, 2289–2292.
58 A. Saravanan, P. S. Kumar, S. Karishma, D.-V. N. Vo, S. Jeevanantham, P. R. Yaashikaa and C. S. George, A review on biosynthesis of metal nanoparticles and its environmental applications, *Chemosphere*, 2021, **264**, 128580.
59 B.-K. Pong, H. I. Elim, J.-X. Chong, W. Ji, B. L. Trout and J.-Y. Lee, New Insights on the Nanoparticle Growth Mechanism in the Citrate Reduction of Gold(III) Salt: Formation of the Au Nanowire Intermediate and Its Nonlinear Optical Properties, *J. Phys. Chem. C*, 2007, **111**, 6281–6287.
60 P. Vanýsek, in *CRC Handbook of Chemistry and Physics*, ed. W. M. Haynes, 92nd edn, 2011.
61 M. H. Sayadi, N. Salmani, A. Heidari and M. R. Rezaei, Bio-synthesis of palladium nanoparticle using Spirulina platensis alga extract and its application as adsorbent, *Surf. Interfaces*, 2018, **10**, 136–143.
62 M. Hekmati, F. Bonyasi, H. Javaheri and S. Hemmati, Green synthesis of palladium nanoparticles using Hibiscus sabdariffa L. flower extract: Heterogeneous and reusable nanocatalyst in Suzuki coupling reactions, *Appl. Organomet. Chem.*, 2017, **31**, e3757.
63 M. Nasrollahzadeh, S. M. Sajadi, E. Honarmand and M. Maham, Preparation of palladium nanoparticles using Euphorbia thymifolia L. leaf extract and evaluation of catalytic activity in the ligand-free Stille and Hiyama cross-coupling reactions in water, *New J. Chem.*, 2015, **39**, 4745–4752.
64 R. Nudelman, S. Zuarets, M. Lev, S. Gavrieli, L. Meshi, I. Zucker and S. Richter, One-pot green bio-assisted synthesis

of highly active catalytic Palladium nanoparticles in Porcine Gastric Mucin for environmental applications, *Nanoscale Adv.*, 2023, **5**(22), 6115–6122.

65 A. Borovik, V. Karanikola and I. Zucker, Platform selection of engineered nanomaterials for water decontamination applications, *Environ. Sci.: Nano*, 2020, **7**, 3641–3654.

66 A. Tressaud, S. Khairoun, H. Touhara and N. Watanabe, X-Ray Photoelectron Spectroscopy of Palladium Fluorides, *Z. Anorg. Allg. Chem.*, 1986, **540**, 291–299.

67 Y.-H. Huang, Y.-F. Huang, C. Huang and C.-Y. Chen, Efficient decolorization of azo dye Reactive Black B involving aromatic fragment degradation in buffered Co2+/PMS oxidative processes with a ppb level dosage of Co2+-catalyst, *J. Hazard. Mater.*, 2009, **170**, 1110–1118.

68 Y. Wang, S. Hui, S. Zhan, R. Djellabi, J. Li and X. Zhao, Activation of peroxymonosulfate by novel Pt/Al2O3 membranes via a non-radical mechanism for efficient degradation of electron-rich aromatic pollutants, *Chem. Eng. J.*, 2020, **381**, 122563.

69 O. S. Furman, A. L. Teel and R. J. Watts, Mechanism of Base Activation of Persulfate, *Environ. Sci. Technol.*, 2010, **44**, 6423–6428.

70 S. Rovani, J. J. Santos, S. N. Guilhen, P. Corio and D. A. Fungaro, Fast, efficient and clean adsorption of bisphenol-A using renewable mesoporous silica nanoparticles from sugarcane waste ash, *RSC Adv.*, 2020, **10**, 27706–27712.

71 H. V. Lutze, N. Kerlin and T. C. Schmidt, Sulfate radical-based water treatment in presence of chloride: Formation of chlorate, inter-conversion of sulfate radicals into hydroxyl radicals and influence of bicarbonate, *Water Res.*, 2015, **72**, 349–360.

72 J. Cong, G. Wen, T. Huang, L. Deng and J. Ma, Study on enhanced ozonation degradation of para-chlorobenzoic acid by peroxymonosulfate in aqueous solution, *Chem. Eng. J.*, 2015, **264**, 399–403.

73 X. Ju, K. Igarashi, S. Miyashita, H. Mitsuhashi, K. Inagaki, S. Fujii, H. Sawada, T. Kuwabara and A. Minoda, Effective and selective recovery of gold and palladium ions from metal wastewater using a sulfothermophilic red alga, Galdieria sulphuraria, *Bioresour. Technol.*, 2016, **211**, 759–764.

74 S. Gavriely, T. Gulakhmedova, Y. Yecheskel, A. E. Rubin, B. Xing, S. Richter and I. Zucker, Slow release of copper from jellyfish-based hydrogels for soil enrichment, *NanoImpact*, 2022, **27**, 100417.

75 J. E. Purcell, E. J. Baxter and V. L. Fuentes, *Jellyfish as products and problems of aquaculture, Advances in aquaculture hatchery technology*, Woodhead Publishing, 2013, pp. 404–430.

